

## Mantle layering across central South America

Kelly H. Liu and Stephen S. Gao

Department of Geology, Kansas State University, Manhattan, Kansas, USA

Paul G. Silver

Department of Terrestrial Magnetism, Carnegie Institution of Washington, Washington, DC, USA

Yongkai Zhang<sup>1</sup>

Department of Geology, Kansas State University, Manhattan, Kansas, USA

Received 17 September 2002; revised 15 May 2003; accepted 23 July 2003; published 1 November 2003.

[1] Imaging of seismic velocity discontinuities along a 3000 km profile across central South America at 20°S suggests that the depth variations of the 410-km (d410) and 660-km (d660) discontinuities are closely associated with the high-velocity Nazca slab and juxtaposed low-velocity oceanic mantle beneath the slab. The mantle transition zone thickness ranges from 220 km in the oceanic mantle to 270 km in a 600-km-wide area occupied by the deflected Nazca slab. The slab deflection has also been suggested by previous studies of seismic tomography and seismicity. This 50 km difference in the thickness corresponds to a lateral temperature variation of about 370°C between the two areas. The depth of d410 shows a gradual eastward decrease of about 10 km along the profile, corresponding to a temperature that is about 75°C cooler to the east. This variation is probably related to changes in the upper mantle geotherms associated with the transition from tectonically active to stable upper mantle. A low-velocity anomaly in the upper mantle and mantle transition zone beneath eastern Brazil, previously detected by seismic tomography and interpreted as a fossil plume, produced no detectable perturbation in transition zone thickness. It is thus unlikely to extend to the transition zone or alternatively is not thermal in origin. Finally, we have observed several possible second-order discontinuities at the depths of 230, 500, 600, 840, and 915 km beneath the western part of the study area.

**INDEX TERMS:** 7218 Seismology: Lithosphere and upper mantle; 7207 Seismology: Core and mantle; 8121 Tectonophysics: Dynamics, convection currents and mantle plumes; **KEYWORDS:** mantle discontinuities, subduction, 410, 660, Nazca

**Citation:** Liu, K. H., S. S. Gao, P. G. Silver, and Y. Zhang, Mantle layering across central South America, *J. Geophys. Res.*, 108(B11), 2510, doi:10.1029/2002JB002208, 2003.

### 1. Introduction

#### 1.1. Tectonic Background

[2] The convergent boundary between the Nazca and South American plates represents one of the major plate boundaries of the global plate tectonics system (Figure 1). The Nazca plate converges with South America at a rate of about 8.5 cm/yr [DeMets *et al.*, 1990] and is subducted at an angle of about 30° [Cahill and Isacks, 1992]. Although subduction in this region is several hundred million years old [Dalziel, 1997], Andean uplift began at approximately 100 Ma, with the latest major episode of uplift beginning around 25 Ma [Isacks, 1988; Allmendinger *et al.*, 1997]. Seismic tomography studies using teleseismic body waves [e.g., Widiyantoro, 1997; Grand, 1994; Engdahl *et al.*, 1995; Dorbath *et al.*, 1996; Dorbath, 1997], local earthquakes

[e.g., Masson *et al.*, 2000], surface waves [e.g., Vdovin *et al.*, 1999; van der Lee *et al.*, 2001], and active source reflection seismology [e.g., Giese *et al.*, 1999] reveal the existence and geometry of the subducted Nazca slab (Figure 2). In central South America (around 20°S), tomographic images suggest that the subducted slab appears to be deflected horizontally by the 660-km discontinuity, and that the oceanic mantle beneath the slab corresponds to a low-velocity zone from the surface to about 660 km (Figure 2). The vast majority of deep earthquakes are in a narrow zone in the depth range 520–620 km, and there is a complete lack of earthquakes in the depth range 325–520 km [Cahill and Isacks, 1992]. Earthquakes in the deflected segment of the slab are rare; during the 32-year period from 1970 to 2001, there was only one earthquake with magnitude  $\geq 5.5$  occurred in the deflected slab (28 February 1989, magnitude 5.6, location 61.465°W, 23.113°S, depth 569 km).

[3] The eastern part of the continent, by contrast, is geologically stable [Riccomini and Assumpção, 1999]. While it is underlain by a cratonic root, it has been shown that there is, in the mantle beneath eastern Brazil, a low-

<sup>1</sup>Now at Department of Civil and Environmental Engineering, University of California, Berkeley, California, USA.

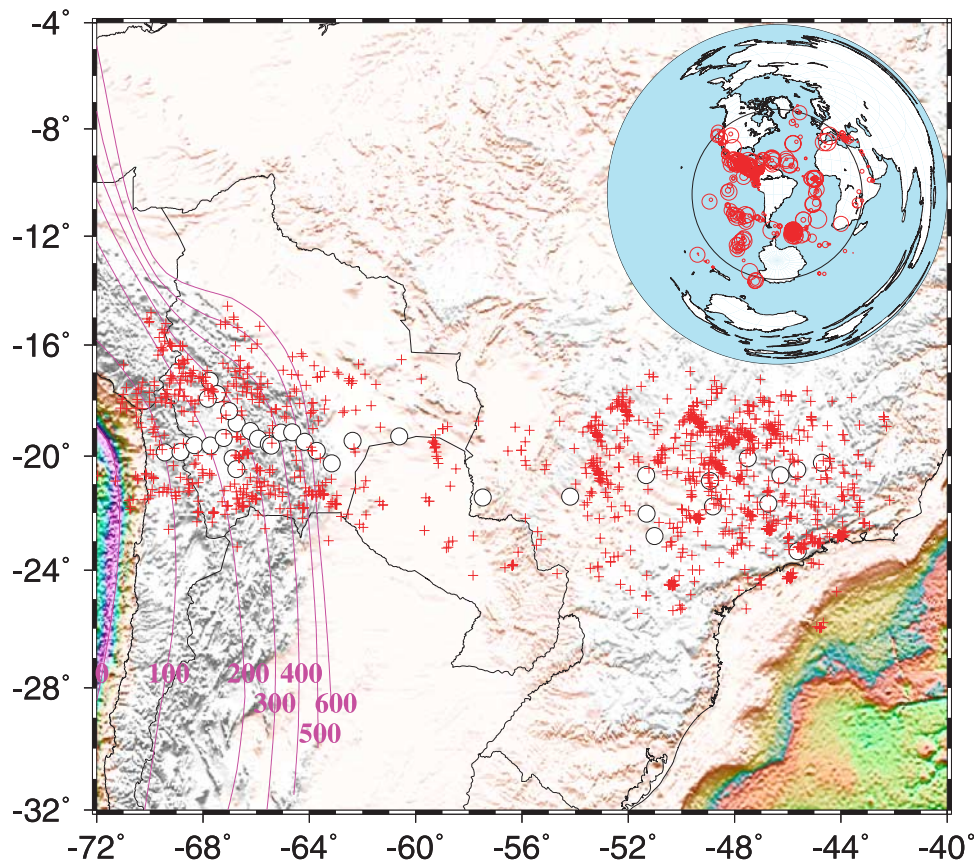


**Figure 1.** A map of the study region showing topographic relief, ray piercing point locations at 660 km depth (crosses), stations used in the study (open circles), and contours of the subducting Nazca slab based on seismicity (purple lines [Gudmundsson and Sambridge, 1998]). The inset at the top right corner shows the location of the events used in the study. The size of a circle is proportional to the number of teleseismic  $P$  wave records used from the event.

velocity feature [VanDecar *et al.*, 1995]. It is approximately centered at (49°W, 21°S) with a characteristic dimension of 300 km and has been interpreted as a fossil plume that has remained geographically fixed with respect to the overlying continent since the opening of the Atlantic Ocean at about 125 Ma. This same low-velocity feature can also be seen on several other tomographic images such as that of Widiyantoro [1997] (Figure 2) and van der Lee *et al.* [2001]. The low velocity was considered to be the result of a thermal anomaly of about 200°C, possibly combined with a compositional anomaly [VanDecar *et al.*, 1995].

## 1.2. Mantle Discontinuities

[4] The 410- and 660-km discontinuities (hereinafter referred to as d410 and d660, respectively) are the two most significant and best observed seismic reflectors in the mantle. The seismologically observable topography of d410 and d660 provides direct information about the temperature in the mantle transition zone (MTZ) and adjacent part of the mantle and thus constitutes an important constraint on geodynamic and geochemical models for mantle processes. High-pressure experiments in mineral physics and numerical modeling suggest that d410 is caused by the phase transition of  $(\text{Mg}, \text{Fe})_2\text{SiO}_4$  (olivine) to its high-pressure polymorph  $\beta$ -spinel (wadsleyite), and d660 is mainly due to the phase transition of  $\gamma$ -spinel (ringwoodite) to  $\text{MgSiO}_3$  (perovskite) and  $(\text{Mg}, \text{Fe})\text{O}$  (magnesiowustite) [e.g., Liu,

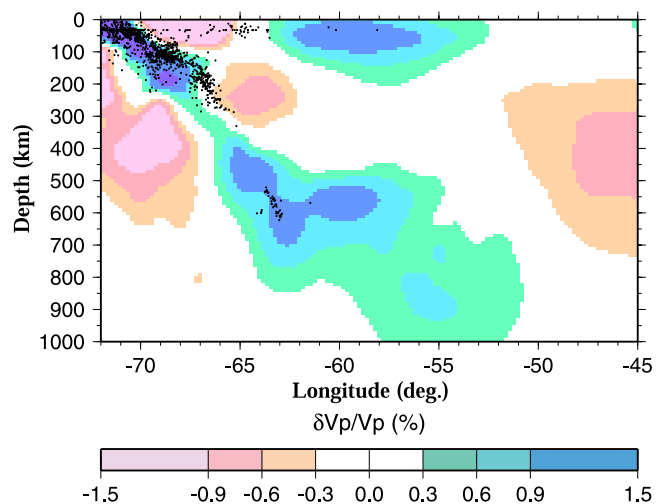


**Figure 2.** Result of seismic tomography [Widiyantoro, 1997] across the profile approximately along 20°S. Dots are locations of magnitude  $\geq 5.5$  earthquakes that occurred during 1970–2001 in the latitude range 16°S–30°S, in which the slab dips mostly to the east. The low-velocity feature in the mantle to the east has been interpreted as a fossil mantle plume [VanDecar *et al.*, 1995].

1976, 1979; Jackson, 1983; Ito *et al.*, 1984; Weidner and Ito, 1987; Ringwood, 1975; Poirier, 1991; Chudinovskikh and Boehler, 2001]. Laboratory results indicate that the Clapeyron slope for d410 is positive and that for d660 is negative, implying that d410 would be uplifted by cold slabs in the MTZ, while d660 would be depressed.

[5] Large topographic variations in both d410 and d660 have been observed beneath subduction zones. For instance, it was found that d410 is uplifted by approximately 30 km in the Izu-Bonin [Collier and Helffrich, 1997] and Tonga [Gilbert *et al.*, 2001] subduction zones, and d660 appears to have been depressed by as much as 70 km in the Izu-Bonin subduction zone [Wicks and Richards, 1993; Castle and Creager, 1998]. A recent study [Gilbert *et al.*, 2001] using *P*-to-*S* converted waves suggests that d660 beneath Tonga was depressed by 20 to 30 km, which is significantly smaller than the 70 km depression obtained using teleseismic *S*-to-*P* conversions [Niu and Kawakatsu, 1995] but is larger than results from *SS* precursor studies which found that d660 is depressed by 15 km [Flanagan and Shearer, 1998a].

[6] There have been a few studies examining mantle discontinuities beneath South America. *SS*, *sS*, *sP*, and *pP* precursor studies [Shearer and Masters, 1992; Flanagan and Shearer, 1998a, 1998b] found an approximately 15 km broad depression of d660 beneath the central part of the South American continent. The same studies found that d410 is normal or even depressed by several km rather than being uplifted near the location where the slab enters the MTZ. Stacking of source-side converted and reflected phases from a deep earthquake in the Nazca subduction zone recorded by the short-period seismic stations in California suggests that the MTZ thickness in the vicinity of the subducted slab is about 280 km [Vidale and Benz, 1992]. The earthquake is located at (62.9°W, 28.7°S), which is about 900 km south of our study region (Figure 1). Using *ScS* reverberations from the 1994 Bolivia earthquake and recorded by some of the stations used in the present study, Clarke *et al.* [1995] estimated the transition zone thickness to be 280–290 km, a value that is most heavily weighted toward the epicenter region of the event, located about 600 km north of our study region. This estimate, like the Vidale and Benz [1992] study, is significantly larger than the global average and likely indicates the presence of a cold descending slab.

[7] This study represents the first systematic investigation of spatial variations in the MTZ and other discontinuities across the South American continent, with a resolution that is several times higher than previous continental- or global-scale studies. It represents an opportunity to study the behavior of mantle discontinuities in a convergent margin setting, and then to follow this behavior into a stable cratonic area to the other edge of the continent.

## 2. Data

[8] Stacking of a large amount of *P*-to-*S* converted phases (*PdS* using convention of Clarke and Silver [1991]) to image mantle discontinuities has recently become a standard technique [Gurrola *et al.*, 1994; Dueker and Sheehan, 1998; Li *et al.*, 1998; Gilbert *et al.*, 2001; Gao *et al.*, 2002]. *PdS* has a Fresnel zone that is significantly smaller than that of the phases used by most of the previous studies conducted in central South America, because those studies used long

period waves, bounce point phases (such as *SS*), or both. The effect of subducting slabs on transition zone discontinuities can be most effectively evaluated by stacking *PdS* recorded by a local network directly above the subducted slab, with a station spacing that is several times smaller than the expected width of the area in the MTZ affected by the cold slab. Furthermore, the network should extend well beyond the area influenced and complicated by subduction, so that a stable reference can be provided. Thus far, the only existing data set to our knowledge that satisfies all of these requirements is a combined data set of three portable broadband seismic experiments conducted in South America (Figure 1), which formed a nearly 3000 km long E-W profile across the entire continent at 20°S. Those experiments include Broadband Andean Joint experiment (BANJO), Seismological Examination of the Deep Altiplano (SEDA) [Beck *et al.*, 1994], and Brazil Lithospheric Seismic Program (BLSP) [James *et al.*, 1993]. About 40 sites were occupied by three-component broadband seismometers (Figure 1). Hundreds of earthquakes were recorded by the array with excellent quality. Previous studies, mostly using one or two of the three data sets, revealed the existence of seismic anisotropy related to both mantle flow [Polet *et al.*, 2000] and ancient tectonics [James and Assumpção, 1996]. A low-velocity anomaly was detected beneath Brazil using *P* and *S* wave travel time tomography, which was interpreted as a fossil plume [VanDecar *et al.*, 1995]. An *ScS* reverberation study indicates the existence of the 210, 410, and 660 km discontinuities [Clarke *et al.*, 1995]. *P*-to-*S* converted phases recorded by BANJO, SEDA, and others were used to study the geometry and velocity contrast of the subducted slab in the top 200 km beneath the Andes [Yuan *et al.*, 2000]. In addition, several studies were conducted using the data set to examine the great Bolivia deep earthquake of June 9, 1994 [Silver *et al.*, 1995; Jiao *et al.*, 1995; Beck *et al.*, 1995; Myers *et al.*, 1998].

[9] We have reprocessed the various data sets into a uniform format, and selected records from events with epicentral distance between 30° to 95°. The seismograms were then converted to receiver functions using the procedure of Ammon *et al.* [1990]. We use factor,  $R = A_{\text{coda}}/A_p$ , where  $A_{\text{coda}}$  is the maximum amplitude in the time window starting from 20 s after the first arrival to the end of the receiver function, and  $A_p$  is the amplitude of the first *P* arrival, to control the quality of the receiver functions. A receiver function is not used if  $R > 2/3$ . A total of about 2100 radial receiver functions from about 500 teleseismic events are used for the stacking. In Figure 3 the radial receiver functions are grouped into 1° bins according to their depth-corrected epicentral distances, and those in the same bins are then stacked in the time domain. While the eastern region shows clear *PdS* of the first-order discontinuities (the Moho, d410, and d660), those arrivals are more scattered on the western region, suggesting either weak discontinuities, or significant spatial variation in their depths. In addition, *P660S* arrives several seconds later than the predicted time, which implies an MTZ that is on average thicker than 250 km (the MTZ thickness in IASP91) beneath the western region.

## 3. Method

[10] The stacking technique that we have utilized is the common conversion point procedure [Dueker and Sheehan,

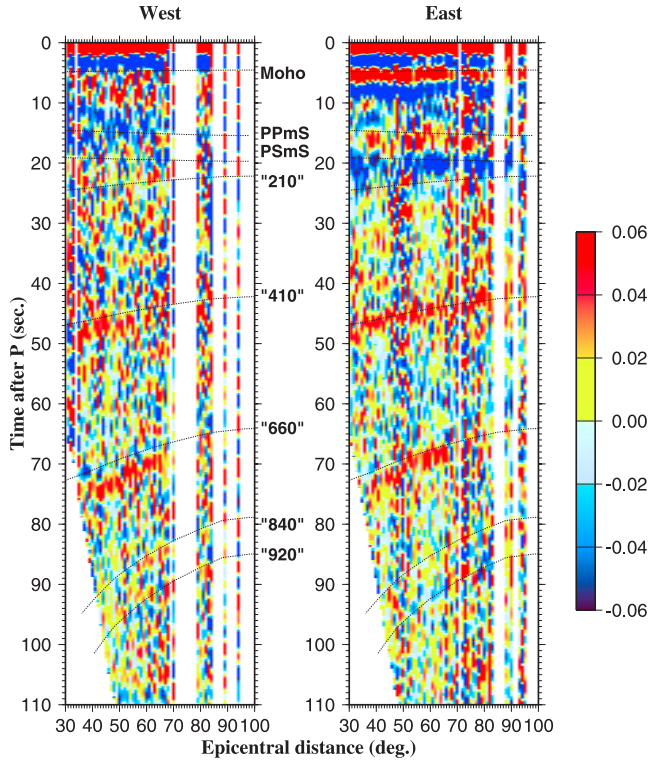


**Figure 3.** Binned and stacked radial receiver functions in the frequency band 0.01–0.2 Hz for the western and eastern regions, divided at 55°W. Receiver functions are binned according to their depth-corrected epicentral distances into 1° bins and those in the same bins are then stacked. The dashed lines are predicted moveout curves for  $PdS$  phases from discontinuities at 35, 210, 410, 660, 840, and 920 km, as well as two Moho reverberation phases,  $PP\dot{m}S$  and  $PS\dot{m}S$ , based on the IASP91 Earth model.

1998]. It constitutes the stacking of  $P$ -to- $S$  converted phases according to predicted  $PdS$  arrival times calculated using [Sheriff and Geldart, 1993; Gurrola et al., 1994; Dueker and Sheehan, 1998]

$$T_{PdS} = \int_{-d}^0 \left[ \sqrt{V_s(z)^2 - p^2} - \sqrt{V_p(z)^2 - p^2} \right] dz, \quad (1)$$

where  $p$  is the ray parameter for the  $P$  wave,  $d$  is the depth of the candidate discontinuity, and  $V_p(z)$  and  $V_s(z)$  are the  $P$  and  $S$  wave velocities, respectively, at depth  $z$ . The receiver functions, which are time series, are then stacked and converted to depth series using

$$A(d) = \frac{1}{N} \sum_{i=1}^N A_i(T_{PdS}^{(i)}), \quad (2)$$

where  $A(d)$  is the stacking amplitude for a candidate discontinuity at depth  $d$ ,  $N$  is the number of traces (i.e., the number of ray-piercing points of qualified receiver functions at depth  $d$ ),  $T_{PdS}^{(i)}$  is the  $PdS$  moveout time of the  $i$ th receiver function for a discontinuity computed using equation (1), and  $A_i(T_{PdS}^{(i)})$  is the amplitude of the  $i$ th receiver function at time  $T_{PdS}^{(i)}$ . In equation (2) the reference time for each trace is the time of the first  $P$  arrival.

[11] The procedure includes the following steps: (1) filtering broadband seismograms in a series of frequency bands and computing radial receiver functions from teleseismic  $P$  waves; (2) computing the geographic locations of the ray-piercing points of all the high-quality receiver functions at each of the candidate depths, by tracing the rays through a 1-D velocity model; (3) calculating the moveout at each candidate depth for each receiver function using equation (1); (4) dividing the study region into rectangular areas; and (5) stacking the moveout-corrected receiver functions within the same rectangular area using equation (2) to produce depth images of the discontinuities. Note that for a given area, the number of ray-piercing points usually changes with depth due to the lateral variation of the location of the points with depth. In this study we use the  $V_p(z)$  and  $V_s(z)$  values in the IASP91 Earth model [Kennett and Engdahl, 1991], and therefore all the depths are relative to IASP91. Results can be easily converted to the “true” depths using a local velocity model. The candidate depths have an increment of 1 km, and range from 0 to 1000 km. In principle the use of a 3-D velocity model such as the one shown in Figure 2 would lead to more realistic results. Given the small magnitude of velocity variations in the transition zone, which is the focus of our study, we estimated that the use of a 3-D model would at the maximum result in a change of a few kilometers in the resulting transition zone thickness. If a correction for the high velocity anomalies associated with the slab in the MTZ is performed, the resulting MTZ thickness would be about 2 km thicker than what is observed (see Figure 6). In addition, the currently available velocity models for the study region [e.g., Grand, 1994; Engdahl et al., 1995; Widiantoro, 1997; van der Lee et al., 2001] show considerable inconsistencies with each other. Those factors, together with the enormous computing time for 3-D ray tracing, promoted our use of the IASP91 Earth model. The use of a 1-D model is sufficient to map long-wavelength variations of discontinuity depth, and could produce distorted images of the discontinuities near regions of short-wavelength structures. However, because of the large (a few hundred kilometers) Fresnel zone of the  $P$ -to- $S$  converted phases at  $d410$  and  $d660$ , structures with a wavelength shorter than the width of the Fresnel zone will be smoothed out and cannot be imaged by the technique. To estimate the degree of distortion of the discontinuities related to velocity heterogeneities, we compare the horizontal locations of the ray-piercing points calculated based on the IASP91 Earth model and a model that represents the extreme velocity anomalies from seismic tomography shown in Figure 2, and conclude that the distortion due to the use of the 1D model is insignificant. For instance, for an epicentral distance of 60°, the horizontal distance calculated based on the IASP91 Earth model between the station and the conversion point is 254.0 km at a depth of 700 km. On the basis of a model with 2% velocity anomaly from 410 to 670 km, the distance is 256.4 km.

[12] We use the bootstrap method [Press et al., 1992; Efron and Tibshirani, 1986] to estimate the standard deviations of the discontinuity depths. For each bootstrap step, we randomly choose  $1 - 1/e = 63\%$  independent receiver functions from the original data set. About 60% of the chosen ones are then duplicated so that the total number of the new set of receiver functions is the same as that of the

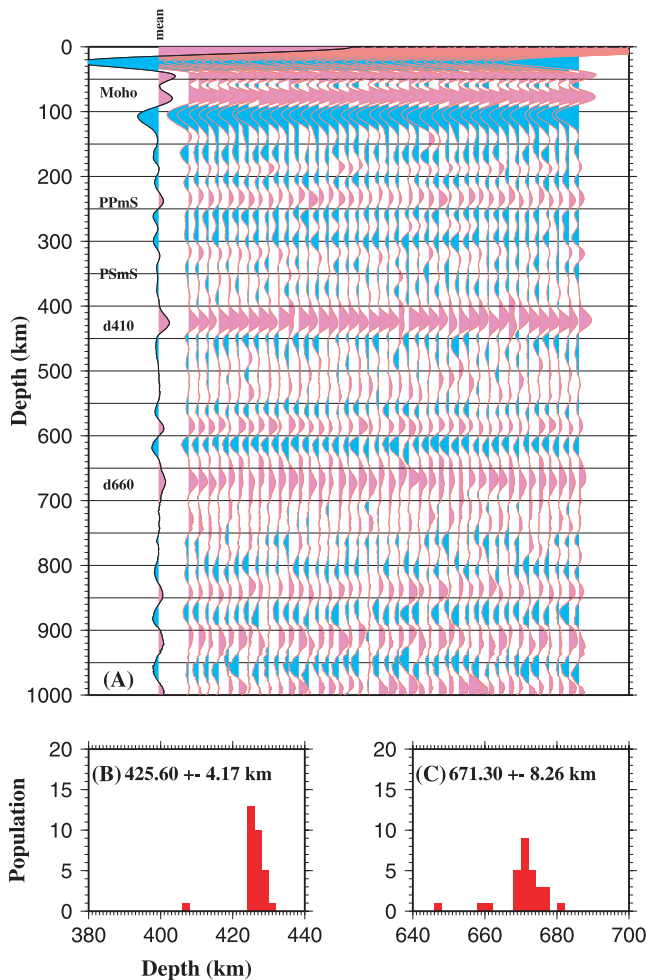


**Figure 4.** Results of the bootstrap resampling procedure for one of the rectangular areas ( $66.5^{\circ}\text{W}$ – $69^{\circ}\text{W}$ ). (a) discontinuity images from 40 bootstrap resamplings for this area. The trace on the left is the mean of the 40 traces on its right. (b) Histogram of the depths of d410 from the resamplings. (c) histogram of the depths of d660. The depths to the discontinuities are relative to the IASP91 Earth model.

original set. Equations (1) and (2) are used on the new set of receiver functions to produce images of discontinuities. The resulting estimated depth of a particular discontinuity is expected to be distributed around the true depth [Press *et al.*, 1992]. The process is repeated and the standard deviation for any given discontinuity can then be estimated. Figure 4 shows an example of the bootstrap procedure for one of the rectangular areas.

## 4. Results

### 4.1. Global Stacking

[13] Using the technique described above, we stack receiver functions with ray piercing points in the regions west and east of the  $55^{\circ}\text{W}$  longitudinal line separately for the purpose of detecting first-order differences in the existence, sharpness, and apparent depth of the discontinuities between the two regions. Above d660, the western region is a heterogeneous area consisting of oceanic and continental mantle and subducted slabs, and the eastern region is mostly

stable craton. Figure 5 shows the results of stacking for a series of frequency bands. Note that for a rectangular area, the number of qualified ray-piercing points may vary with the frequency bands due to variation of the signal-to-noise ratio with frequency. Beneath the western region, the mean depth for the Moho, d410, and d660 is about 70, 420, and 670 km, respectively, and the transition zone thickness is 250 km. Beneath the eastern region, the corresponding values are 40, 410, 650, and 240 km, respectively. In the western region, the Moho multiples show small stacking amplitudes, which is a result of incoherent stacking caused by the significant spatial variation of Moho depth, which ranges from 70 km beneath the central Andes to about 35 km beneath the Chaco plain in the east [Beck *et al.*, 1996]. Both the positive  $PPmS$  and the negative  $PSmS$  are more visible in the eastern region (Figure 5). In the east, the Moho depth from a recent study using data from BLSP [Assumpção *et al.*, 2002] suggests a mean Moho depth of about 41 km, which is consistent with our results (Figure 5d).

[14] Also included in Figure 5 are the results from Complete Ordered Ray Expansion (CORE) [Clarke and Silver, 1991] synthetics with a Moho, d410, and d660 at the approximate observed depths for the eastern and western regions. The velocities in the IASP91 Earth model are adopted, and the same source-receiver geometries are used as in the data set. The Moho and its multiples, as well as d410 and d660, can be seen in the synthetics. Relative to the synthetics, the amplitudes of  $PPmS$  and its multiples in the data are smaller, because spatial variation of Moho depth tends to reduce the stacking amplitude of  $PdS$  and especially its multiples.

[15]  $P$ -to- $S$  conversions from both d410 and d660 can be observed at frequencies up to 0.5 Hz both in the east and west, implying that the sharpness of the discontinuities is 8 km or less, based on the assumption that the discontinuity must be thicker than  $1/2$  of  $P$  wavelength to be observed [Bostock, 1999].

### 4.2. Spatial Variation of Transition Zone Discontinuities

[16] Figure 6 provides an image of discontinuity location across South America for a depth range of 0 to 1000 km. At each depth, receiver functions with piercing points inside the same rectangular area are stacked. Because most of our profile is E-W and the strike of the subducting slab in the study region is approximately N-S, we choose the dimensions of the rectangular area to be  $2.5^{\circ}$  longitudinal units in the E-W direction, and  $12^{\circ}$  in the N-S direction, i.e., we made the assumption that the discontinuity structure is two-dimensional with a N-S strike. The actual N-S dimension depends on the spatial distribution of piercing points, ranging from about 1000 km in the west to about 500 km in the east at the depth of 660 km. The assumption is further supported by the resulting sharp arrivals for both d410 and d660 (Figure 6); significant variations in discontinuity depths along the N-S direction would produce multiple or blurred arrivals.

[17] The candidate depths that we consider range from 0 to 1000 km. The width of the rectangular area (250 km) is comparable with the size of the first Fresnel zone of the  $P$ -to- $S$  converted phases at d410 and d660. The rectangular areas move eastward by  $1^{\circ}$  at each step. Several areas have less than 15 high-quality receiver functions at 660 km depth, and are not used in the study. Results for a total of

24 areas are obtained. The number of ray piercing points per area at 660 km ranges from 16 to 296, with a mean of 146. Given the size of the areas and the step size, nearby stacks are correlated. In principle a strong arrival (signal or noise) on a seismogram will show up on three nearby stacked traces, and the apparent depths of the “discontinuity”

corresponding to the arrival on all the three traces should be similar. However, the stacking amplitude resulting from an arrival on any single seismogram is expected to be small, because of the large number of stacks per area, and the fact that a receiver function is not used in the stacking if  $R > 2/3$ . Therefore only coherent arrivals from many seismograms will produce an image.

[18] The mean depths of d410 and d660 on each trace is obtained using  $\bar{D} = 1/M \sum_{i=1}^M D_i$ , where  $M$  is the number of bootstraps,  $D_i$  is the depth of d410 (d660) corresponding to the maximum stacking amplitude in the  $410 \pm 30$  km ( $670 \pm 40$  km) depth range from the  $i$ th bootstrap. The standard deviations (STD) of the mean depths,  $\sigma_{d410}$  and  $\sigma_{d660}$ , are calculated using  $\sigma = \sqrt{1/(M-1) \sum_{i=1}^M (D_i - \bar{D})^2}$ , where  $\bar{D}$  is the mean depth. The STD for the MTZ thickness is calculated using  $\sigma_{TZ} = \sqrt{\sigma_{d410}^2 + \sigma_{d660}^2}$ . In the study we use  $M = 10$ , which results in a balance between accuracy and computing time. Experiments show that both  $\bar{D}$  and  $\sigma$  are stabilized when  $M \geq 10$ . For most of the rectangular areas,  $\sigma_{d410}$  is significantly smaller than  $\sigma_{d660}$  (Figure 7). This relationship can also be observed in Figure 6, where d410 is sharper than d660 for most of the areas.

[19] Some measurements with multiple arrivals or low signal level are excluded in the discussions below. Those include (1) measurements for d410 on traces  $f$  and  $g$  (Figure 6) due to double arrivals; (2) measurements for d410 and d660 on trace  $k$  due to low signal level; and (3) measurement for d660 on trace  $x$  due to a double arrival. The multiple arrivals may be due to incoherent stacking resulting from velocity heterogeneities.

[20] The depth of d410 ranges from 402 to 429 km with a mean of 416.5 and that of d660 ranges from 650 to 700 km with a mean of 662.5 km. The depth of d410 decreases toward the east at a significant gradient of about  $1.0 \pm 0.2$  km per 100 km (Figure 8), and that of d660 has a slope that is statistically insignificant. In the area where the slab encounters d410 (near  $65^\circ\text{W}$ ) the depth of d410 is reduced by about 10 km relative to both the western and eastern sides (Figure 8). In addition, in the same area, the amplitude of

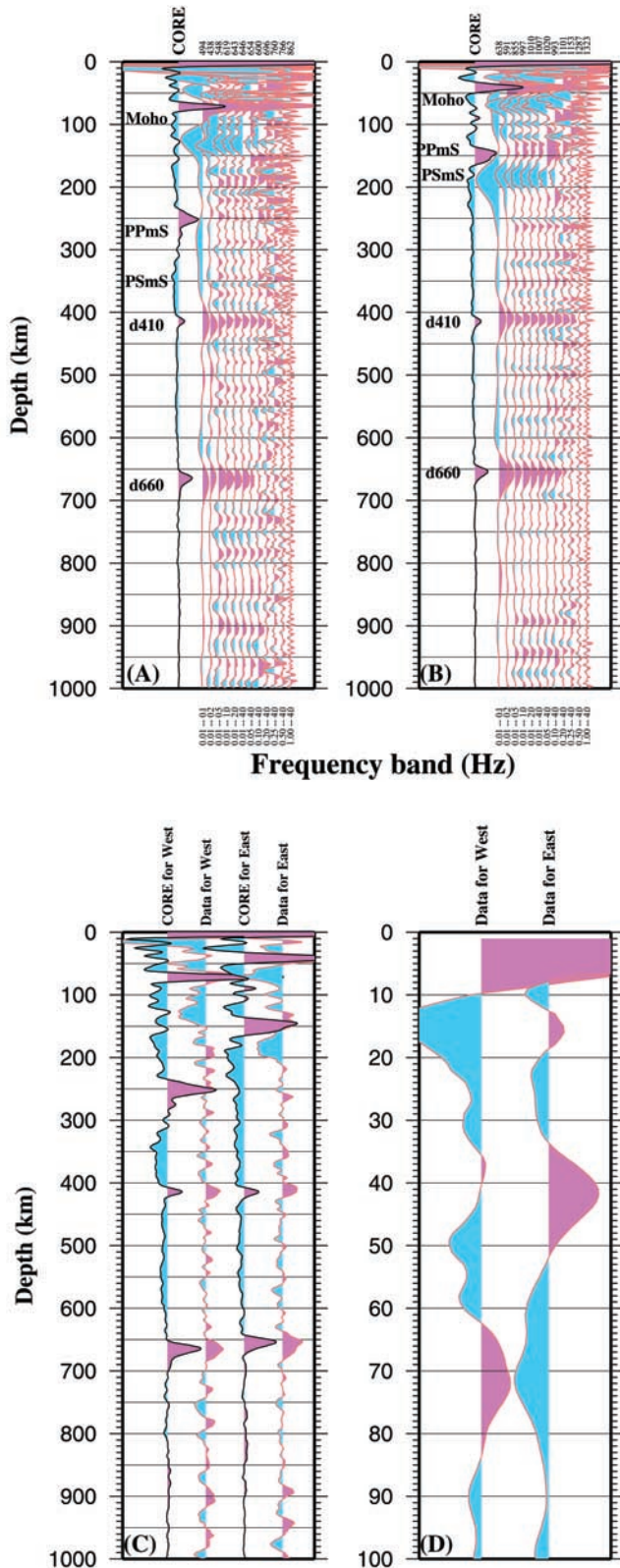


**Figure 5.** (opposite) Discontinuity images for ray piecing points at the (a) west and (b) east of  $55^\circ\text{W}$  for a sequence of frequency bands. The trace on the left side of each panel is derived from CORE synthetics generated using the IASP91 Earth model, which was modified to contain only four discontinuities (the Moho, d410, d660, and the core-mantle boundary). The depth of the discontinuities was modified to reflect the approximate depth for the east and west regions, respectively. Frequency bands are labeled at bottom of the plot. Positive (negative) polarities are shaded in purple (blue). The traces are normalized by the maximum positive amplitude in the depth range from 350 to 450 km. The number of ray piercing points at 660 km depth for each frequency band is shown at the top of the figure. Note consistency and visibility of d410 and d660 even to relatively high frequencies, and significant differences in the depth of the Moho, d410, and d660 between the western and eastern regions. (c) A detailed comparison between the CORE synthetics and observations in the 0.01–1.0 Hz band, and (d) the top 100 km of the observations in the 0.01–1.0 Hz band.

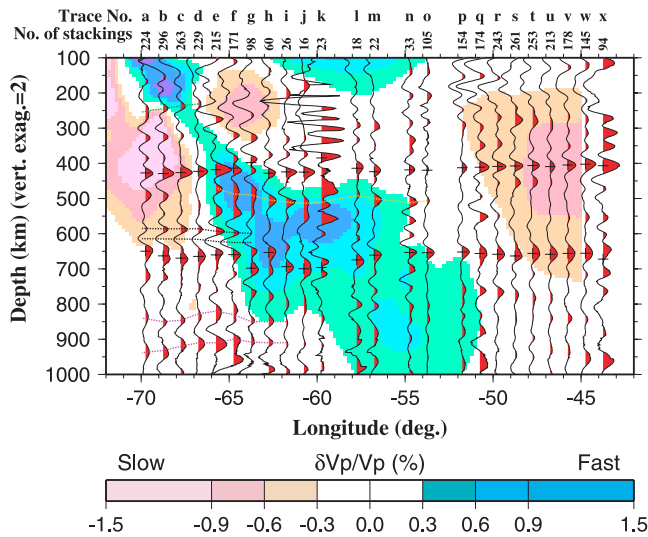


**Figure 6.** Results from stacking of radial receiver functions in the 0.01–0.2 Hz frequency band across South America plotted on top of a  $P$  wave tomographic model across the profile [Widiyantoro, 1997]. The E-W dimension of the rectangular areas is  $2.5^\circ$ , and the N-S dimension is  $12^\circ$ . Positive polarities of the traces are shaded. The traces are normalized by the maximum positive amplitude in the 650–700 km depth range on each trace. The crosses mark the mean depths of d410 and d660 from the bootstrap procedure, the green dashed line in the upper mantle marks a possible tilting discontinuity at about 230 km depth, the yellow dashed line in the MTZ marks a possible interface which may be the top of the deflected slab, and the two purple dashed lines represent two possible discontinuities in the lower mantle. The dark dashed lines indicate a pair of discontinuities near the bottom of the transition zone. The top row above the plot shows area names, and the second row indicates the number of stackings at 660 km depth.

d410 is reduced relative to that of d660 (Figure 6), implying either a weaker velocity contrast in the vicinity of the slab relative to that outside it, or a result of the defocusing effect of the upward curvature of d410. In an approximately 600-km-wide zone (from about  $63^\circ\text{W}$  to  $57^\circ\text{W}$ ), d660 is clearly depressed by the subducted slab by as much as 40 km. Beneath the western end of the profile, the depth of d660 decreases westward at a rate of about 10 km per 100 km, while that of d410 shows little variation.

[21] The MTZ thickness ranges from 220 to 275 km, with a profile mean of 245.3 km. This value is essentially equal to the global average found by Flanagan and Shearer [1998a] and Gu *et al.* [1998] using  $SS$  precursors. It has a slight eastward increase in thickness of about  $0.4 \pm 0.03$  km per 100 km (Figure 8). The oceanic mantle beneath the slab is associated with an anomalously thin MTZ of 220 km. The thickest MTZ, 274 km, is found at about  $61^\circ\text{W}$ .

## 5. Discussion

### 5.1. Slab Deflection and Transition Zone Discontinuities

[22] Stacking of  $PdS$  shows clearly a strong interaction between the subducted Nazca slab and the South American

MTZ discontinuities. The cold slab locally thickens the MTZ by about 40 km. The width of the area is several times larger than the thickness of a typical oceanic slab. The zone of thickened MTZ is comparable in size to the region occupied by the horizontally deflected slab imaged by seismic tomography [e.g., Widiyantoro, 1997; Engdahl *et al.*, 1995], which is also an area with isolated deep earthquakes [Lundgren and Giardini, 1994]. To our knowledge, this is so far the only deflected slab that has been revealed by three independent sources of data. As suggested by Morgan and Shearer [1993], the deflection may be caused by the resistance of the slab by d660. Because the density of the material below d660 is higher than that above it, the thermally induced depression leads to an upward restoring force, which resists the penetration of the slab and deflects it horizontally by several hundred km. In addition to the observation of this deflection, the spatial variation in the amount of thickening can provide a temperature anomaly estimate in this region. Taking the values of Clapeyron slopes to be  $2.9 \text{ MPa}/^\circ\text{K}$  and  $-2.1 \text{ MPa}/^\circ\text{K}$  for d410 and d660, respectively [Bina and Helffrich, 1994], this corresponds to a local MTZ temperature decrease of  $300^\circ\text{C}$ . Not surprisingly the greatest thickness is located at about  $61^\circ\text{W}$  (Figure 8), along the extension of the slab based on seismicity as well as tomography (Figure 2).

### 5.2. Cause of the Eastward Uplift of d410

[23] As mentioned above, the depth of d410 decreases toward the east at a significant gradient of about 0.9 km per

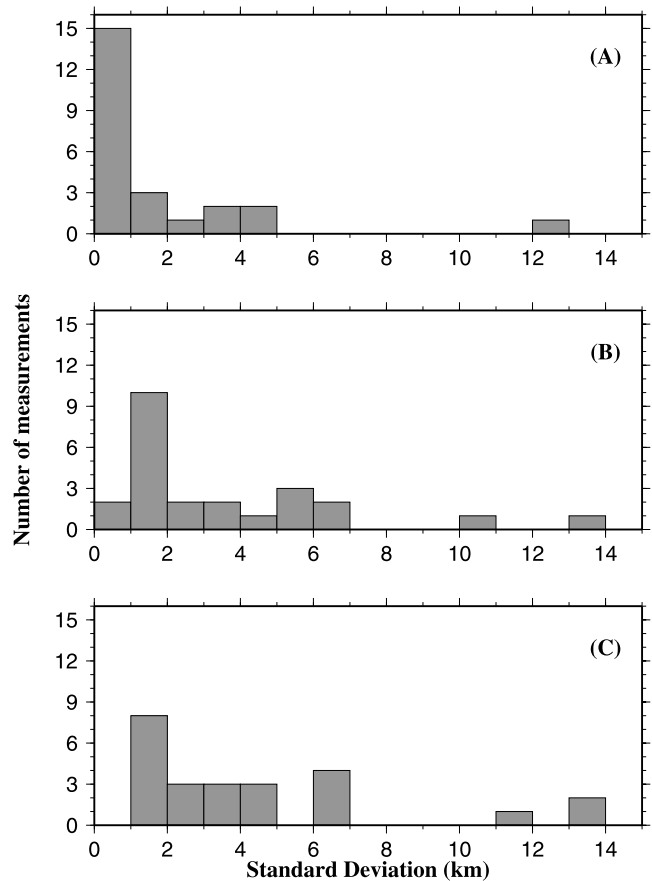


**Figure 7.** Histograms for the standard deviations for (a) the depths of d410; (b) the depth of d660; and (c) thickness from bootstrap method.

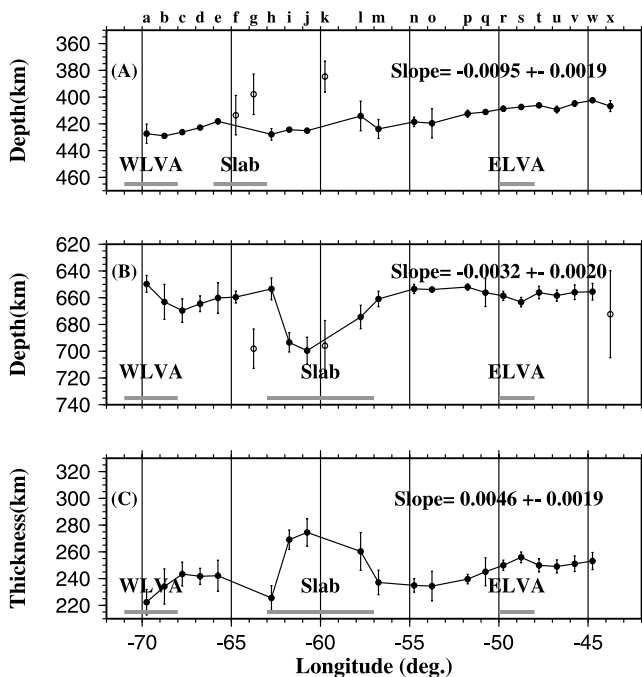


**Figure 8.** Measurements of (a) depth to d410; (b) depth to d660; and (c) thickness of the MTZ from the bootstrap procedure. Solid symbols represent high-quality measurements, and open symbols are those excluded in the discussion because of multiple arrivals or low signal level. The gray bars at the bottom of each panel denote the range of three features in the tomographic model in Figure 6: the slab with velocity anomalies of 0.6% or larger, the eastern low-velocity anomaly (ELVA) [VanDecar *et al.*, 1995] and the western low-velocity anomaly (WLVA). Note thinning of MTZ associated with the WLVA, the dramatic thickening associated with the slab, and the absence of a MTZ perturbation related to the ELVA.

100 km (Figure 8), which is mostly responsible for the modest eastward thickening of the MTZ. Part of the uplift could be apparent, due to a gradual eastward increase in upper mantle velocity above d410. This transect represents a transition from tectonically active to stable continent, as well as a significant change in crustal thickness. Vertical  $S_cS$  travel times using these same stations suggest an upper mantle variation of 3–4% between the eastern and western parts of the profile [Clarke *et al.*, 1995], assuming that the travel time variation is entirely due to upper mantle structure. Vertical integration of the tomographic model in Figure 2 gives a value of about 2%. If all of this gradient were due to upper mantle lateral heterogeneity, however, it would require a larger lateral difference in vertically integrated velocity variation of about 6.3% between the western and eastern ends of the profile. Consequently, about half of this gradient is probably due to upper mantle heterogeneity and half to actual variation in the depth of the boundary. It is thus likely that the upper mantle thermal structure, as reflected in the heterogeneity, has an influence on the geotherm at least into the top of the transition zone. The resulting difference in the depth of d410 across the profile is about 10 km, which, given the value of the Clapeyron slope

of 2.9 MPa/°K [Bina and Helffrich, 1994], is about 120°C. A lateral temperature difference of about 75°C is obtained in the transition zone if we assume that the temperature is vertically coherent throughout the transition zone.

### 5.3. Characteristics of the Oceanic MTZ

[24] The oceanic MTZ beneath the slab is abnormally thin by about 25 km, and would be consistent with a transition zone temperature elevated by about 180°C. Several tomographic studies (see Figure 6 for an example) do show a low-velocity anomaly in the transition zone, although the depth and spatial extent are variable. Some show a low-velocity anomaly in the vicinity of d410, while others suggest a low-velocity zone immediately beneath d660 in the area [see Engdahl *et al.*, 1995, Figure 3e]. A thermal anomaly directly beneath the slab may suggest a cause that is related to the subduction process, such as the slab entrainment of high-temperature material originating from the ridge [e.g., Gu *et al.*, 2001].

### 5.4. Low-Velocity Anomaly Beneath Brazil

[25] Using teleseismic travel time data recorded by BLSP, VanDecar *et al.* [1995] found a low-velocity feature in the upper mantle and MTZ beneath eastern Brazil, and interpreted it as a fossil mantle plume. They suggested that the low velocity is primarily the result of a thermal anomaly of 200°C, with a possible small compositional contribution. The thermal anomaly would have two effects on the apparent thickness of MTZ. The first effect is that the low velocities within the transition zone would lead to an apparent thickening of the MTZ of about 2 km based on either velocity model [VanDecar *et al.*, 1995; Widiyantoro, 1997], which is smaller than most of the standard deviations of the observed discontinuity depths. The second and dominant effect of such a thermal anomaly would be the thinning of the MTZ by about 25 km if both d410 and d660 are affected, or 15 km if only d410 is affected. Thinning of the MTZ is not observed, and if anything, there is a slight thickening. We may thus conclude that either the thermal anomaly does not extend into the transition zone, or alternatively that the observed anomaly is not primarily thermal, and rather dominantly compositional in origin.

### 5.5. Other Candidate Discontinuities

[26] In addition to the arrivals corresponding to d410 and d660, several weaker and less coherent arrivals are observed (Figure 6). CORE synthetics (Figure 5c) clearly suggest that they are not multiples of the Moho, d410, or d660. One of the advantages of this profile is that we have a section that includes both subduction-related and nonsubduction related regions. In fact, all of the candidate discontinuities that we see are on the western side of the profile. One such arrival is found in the region of the deflected slab in the MTZ (Figure 6). The depth of the possible discontinuity ranges from 470 to 514 km, with a mean of 500 km. The arrival could be associated with the top of the deflected slab, which represents a transition from lower to higher velocity. A positive/negative pair of discontinuities are found near the bottom of the transition zone over several rectangular areas at the western end of the profile, at the depths of 590/615 km (Figure 6). Both discontinuities deepen toward

the east. One of the possible causes for such a double-lobed structure is a high-velocity layer of about 25 km thick in the depth range of 590 to 615 km. The layer could be a subducted oceanic slab trapped on top of d660.

[27] Two other candidate discontinuities are seen, one with depth range 820–850 km, with a mean depth of 839 km, and one with range from 900 to 938 km, with a mean of 915 km (Figure 6). The stacking amplitudes of these two lower mantle discontinuities are about half of that of d660, suggesting a velocity contrast of about 3%. To our knowledge, the only previous study that suggested a possible discontinuity at 840 km is by Shearer [1990], based on stacking of SS precursors. The existence of a discontinuity at the depth near 920 km, has, in contrast, been suggested by many studies, although the critical questions regarding whether it is a global or regional feature, as well as its cause, have not been resolved [e.g., Kawakatsu and Niu, 1994]. The fact that we see it in close proximity to subducted slabs in the west but not the east (where slabs are unlikely to be) suggests that this is a regional rather than a global feature. Indeed, so far the best examples of the 920 km discontinuity were found in the vicinity of subduction zones [Kawakatsu and Niu, 1994; Petersen et al., 1993; Revenaugh and Jordan, 1991]. There remains the possibility that this feature is related to oceanic upper mantle, rather than to slabs. This possibility cannot be excluded with the present data set, but can be tested in oceanic regions that are far from a descending slab.

[28] Finally, there appears to be a weak discontinuity at about 230 km in the four areas at the western end of the profile. This could correspond to the discontinuity at about 210 km depth observed by Clarke et al. [1995], based on ScS reverberations beneath an area that is several hundred km north of our study region. The stacking amplitude of this discontinuities is about 1/2 of that of d410 (Figure 6), suggesting that it has a velocity contrast of about 2–3%.

[29] **Acknowledgments.** We would like to thank our colleagues from CIW (D. James, R. Kuehnel), University of Arizona (S. Beck, S. Myers, T. Wallace), LLNL (G. Zandt), and the University of Sao Paulo (M. Assumpção) for their role in collecting the data. Sri Widiyantoro kindly provided his velocity model for South America. The data analysis work was supported by National Science Foundation grants EAR-00-01000 and EAR-01-07055.

## References

- Allmendinger, R. W., T. E. Jordan, S. M. Kay, and B. L. Isacks, The evolution of the Altiplano-Puna plateau of the central Andes, *Annu. Rev. Earth Planet. Sci.*, **25**, 139–174, 1997.
- Ammon, C. J., G. E. Randall, and G. Zandt, On the nonuniqueness of receiver function inversions, *J. Geophys. Res.*, **95**, 15,303–15,318, 1990.
- Assumpção, M., D. James, and A. Snoke, Crustal thicknesses in SE Brazilian Shield by receiver function analysis: Implications for isostatic compensation, *J. Geophys. Res.*, **107**(B1), 2006, doi:10.1029/2001JB000422, 2002.
- Beck, S. L., et al., Across the Andes and along the Altiplano: A passive seismic experiment, *IRIS Newsl.*, **13**(3), 1–3, 1994.
- Beck, S. L., P. Silver, T. C. Wallace, and D. James, Directivity analysis of the deep Bolivian earthquake of June 9, 1994, *Geophys. Res. Lett.*, **22**, 2257–2260, 1995.
- Beck, S. L., G. Zandt, S. C. Myers, T. C. Wallace, P. G. Silver, and L. Drake, Crustal-thickness variations in the central Andes, *Geology*, **24**, 407–410, 1996.
- Bina, C. R., and G. Helffrich, Phase transition Clapeyron slopes and transition zone seismic discontinuity topography, *J. Geophys. Res.*, **99**, 15,853–15,860, 1994.
- Bostock, M. G., Seismic waves converted from velocity gradient anomalies in the Earth's upper mantle, *Geophys. J. Int.*, **138**, 747–756, 1999.
- Cahill, T., and B. L. Isacks, Seismicity and shape of the subducted Nazca plate, *J. Geophys. Res.*, **97**, 17,503–17,529, 1992.
- Castle, J. C., and K. C. Creager, Topography of the 660-km seismic discontinuity beneath Izu-Bonin: Implications for tectonic history and slab deformation, *J. Geophys. Res.*, **103**, 12,511–12,527, 1998.
- Chudinovskikh, L., and R. Boehler, High-pressure polymorphs of olivine and the 660-km seismic discontinuity, *Nature*, **411**, 574–577, 2001.
- Clarke, T. J., and P. G. Silver, A procedure for the systematic interpretation of body wave seismograms; I; Application to Moho depth and crustal properties, *Geophys. J. Int.*, **104**, 41–72, 1991.
- Clarke, T. J., P. G. Silver, Y. L. Yeh, D. E. James, T. C. Wallace, and S. L. Beck, Close in SCS and sSCS reverberations from the 9 June 1994 Bolivian earthquake, *Geophys. Res. Lett.*, **22**, 2313–2316, 1995.
- Collier, J. D., and G. R. Helffrich, Topography of the 410 and 660 km seismic discontinuities in the Izu-Bonin subduction zone, *Geophys. Res. Lett.*, **24**, 1535–1538, 1997.
- Dalziel, I., Neoproterozoic-Paleozoic geography and tectonics: Review, hypothesis, environmental speculation, *Geol. Soc. Am. Bull.*, **109**, 16–42, 1997.
- DeMets, C., R. G. Gordon, D. E. Argus, and S. Stein, Current plate motions, *Geophys. J. Int.*, **101**, 425–478, 1990.
- Dorbath, C., Mapping the continuity of the Nazca plate through its aseismic part in the Arica Elbow (central Andes), *Phys. Earth Planet. Inter.*, **101**, 163–173, 1997.
- Dorbath, C., and A. Paul, Tomography of the Andean crust and mantle at 20°S: First results of the Lithoscope experiment, *Phys. Earth Planet. Inter.*, **97**, 133–144, 1996.
- Dueker, K. G., and A. F. Sheehan, Mantle discontinuity structure beneath the Colorado Rocky Mountains and High Plains, *J. Geophys. Res.*, **103**, 7153–7169, 1998.
- Efron, B., and R. Tibshirani, Bootstrap methods for standard errors, confidence intervals, and other measures of statistical accuracy, *Stat. Sci.*, **1**, 54–75, 1986.
- Engdahl, E. R., R. D. van der Hilst, and J. Berrocal, Imaging of subducted lithosphere beneath South America, *Geophys. Res. Lett.*, **22**, 2317–2320, 1995.
- Flanagan, M. P., and P. M. Shearer, Global mapping of topography on transition zone velocity discontinuities by stacking SS precursors, *J. Geophys. Res.*, **103**, 2673–2692, 1998a.
- Flanagan, M. P., and P. M. Shearer, Topography on the 410-km seismic velocity discontinuity near subduction zones from stacking of sS, sP, and pP precursors, *J. Geophys. Res.*, **103**, 21,165–21,182, 1998b.
- Gao, S. S., P. G. Silver, K. H. Liu, and Kaapvaal Seismic Group, Mantle discontinuities beneath southern Africa, *Geophys. Res. Lett.*, **29**(10), 1491, doi:10.1029/2001GL013834, 2002.
- Giese, P., E. Scheuber, F. Schilling, M. Schmitz, and P. Wigger, Crustal thickening processes in the Central Andes and the different natures of the Moho-discontinuity, *J. S. Am. Earth Sci.*, **12**, 201–220, 1999.
- Gilbert, H. J., A. F. Sheehan, D. A. Wiens, K. G. Dueker, L. M. Dorman, J. Hildebrand, and S. Webb, Upper mantle discontinuity structure in the region of the Tonga Subduction Zone, *Geophys. Res. Lett.*, **28**, 1855–1858, 2001.
- Grand, S., Mantle shear structure beneath the Americas and surrounding oceans, *J. Geophys. Res.*, **99**, 11,591–11,621, 1994.
- Gu, Y., A. M. Dziewonski, and C. B. Agee, Global de-correlation of the topography of transition zone discontinuities, *Earth Planet. Sci. Lett.*, **157**, 57–67, 1998.
- Gu, Y. J., A. M. Dziewonski, W. J. Su, and G. Ekstrom, Models of the mantle shear velocity and discontinuities in the pattern of lateral heterogeneities, *J. Geophys. Res.*, **106**, 11,169–11,199, 2001.
- Gudmundsson, O., and M. Sambridge, A regionalized upper mantle (RUM) seismic model, *J. Geophys. Res.*, **103**, 7121–7136, 1998.
- Gurrola, H., J. B. Minster, and T. Owens, The use of velocity spectrum for stacking receiver functions and imaging upper mantle discontinuities, *Geophys. J. Int.*, **117**, 427–440, 1994.
- Isacks, B. L., Uplift of the central Andean plateau and bending of the Bolivian orocline, *J. Geophys. Res.*, **93**, 3211–3231, 1988.
- Ito, E., E. Takahashi, and Y. Matsui, The mineralogy and chemistry of the lower mantle: An implication of the ultrahigh-pressure phase relations in the system MgO-FeO-SiO<sub>2</sub>, *Phys. Earth Planet. Inter.*, **67**, 238–248, 1984.
- Jackson, I., Some geophysical constraints on the chemical composition of the Earth's lower mantle, *Earth Planet. Sci. Lett.*, **62**, 91–103, 1983.
- James, D. E., and M. Assumpção, Tectonic implications of S-wave anisotropy beneath SE Brazil, *Geophys. J. Int.*, **126**, 1–10, 1996.
- James, D. E., M. Assumpção, J. A. Snoke, L. C. Ribotta, and R. Kuehnel, Seismic studies of continental lithosphere beneath SE Brazil, *Ann. Acad. Bras. Ci.*, **65**, suppl. 2, 227–250, 1993.
- Jiao, W. J., T. C. Wallace, S. L. Beck, P. G. Silver, and G. Zandt, Evidence for static displacements from the June 9, 1994 deep Bolivian earthquake, *Geophys. Res. Lett.*, **22**, 2285–2288, 1995.

- Kawakatsu, H., and F. Niu, Seismic evidence for a 920-km discontinuity in the mantle, *Nature*, 371, 301–305, 1994.
- Kennett, B. L. N., and E. R. Engdahl, Traveltimes for global earthquake location and phase identification, *Geophys. J. Int.*, 105, 429–465, 1991.
- Li, A. B., K. M. Fischer, M. E. Wyssession, and T. J. Clarke, Mantle discontinuities and temperature under the North American continental keel, *Nature*, 395, 160–163, 1998.
- Liu, L.-G., The post-spinel phase of forsterite, *Nature*, 262, 770–772, 1976.
- Liu, L.-G., Phase transformations and the constitution of the deep mantle, in *The Earth: Its Origin, Structure and Evolution*, edited by M. W. McElhinny, pp. 177–202, Academic, San Diego, Calif., 1979.
- Lundgren, P., and D. Giardini, Isolated deep earthquakes and the fate of subduction in the mantle, *J. Geophys. Res.*, 99, 15,833–15,842, 1994.
- Masson, F., C. Dorbath, C. Martinez, and G. Carlier, Local earthquake tomography of the Andes at 20°S: Implications for the structure and building of the mountain range, *J. S. Am. Earth Sci.*, 13, 3–19, 2000.
- Morgan, J. P., and P. M. Shearer, Seismic constraints on mantle flow and topography of the 660-km discontinuity—Evidence for whole-mantle convection, *Nature*, 365, 506–511, 1993.
- Myers, S. C., S. L. Beck, G. Zandt, and T. C. Wallace, Lithospheric-scale structure across the Bolivian Andes from tomographic images of velocity and attenuation for *P* and *S* waves, *J. Geophys. Res.*, 103, 21,233–21,252, 1998.
- Niu, F. L., and H. Kawakatsu, Direct evidence for the undulation of the 660-km discontinuity beneath Tonga—Comparison of Japan and California array data, *Geophys. Res. Lett.*, 22, 531–534, 1995.
- Petersen, N., J. Gossler, R. Kind, K. Stammler, and L. Vinnik, Precursors to *SS* and structure of transition zone of the northwestern Pacific, *Geophys. Res. Lett.*, 20, 281–284, 1993.
- Poirier, J. P., Cloak of mystery over Earth's mantle, *Phys. World*, 4, 26–27, 1991.
- Polet, J., P. G. Silver, S. Beck, T. Wallace, G. Zandt, S. Ruppert, R. Kind, and A. Rudloff, Shear wave anisotropy beneath the Andes from the BANJO, SEDA, and PISCO experiments, *J. Geophys. Res.*, 105, 6287–6304, 2000.
- Press, W. H., S. A. Teukolsky, W. T. Vetterling, and B. P. Flannery, *Numerical Recipes in FORTRAN*, 963 pp., 2nd ed., Cambridge Univ. Press, New York, 1992.
- Revenaugh, J. S., and T. H. Jordan, Mantle layering from *ScS* reverberations: 2. The transition zone, *J. Geophys. Res.*, 96, 19,763–19,780, 1991.
- Riccomini, C., and M. Assumpção, Quaternary tectonics in Brazil, *Episodes*, 22, 221–225, 1999.
- Ringwood, A. E., *Composition and Petrology of the Earth's Mantle*, 604 pp., McGraw-Hill, New York, 1975.
- Shearer, P. M., Seismic imaging of upper-mantle structure with new evidence for a 520-km discontinuity, *Nature*, 344, 121–126, 1990.
- Shearer, P. M., and T. G. Masters, Global mapping of topography on the 660-km discontinuity, *Nature*, 355, 791–796, 1992.
- Sheriff, R. E., and L. P. Geldart, *Exploration Seismology*, 2nd ed., Cambridge Univ. Press, New York, 1993.
- Silver, P. G., S. L. Beck, T. C. Wallace, C. Meade, S. C. Myers, D. E. James, and R. Kuehnel, Rupture characteristics of the deep Bolivian earthquake of 9 June 1994 and the mechanism of deep-focus earthquakes, *Science*, 268, 69–73, 1995.
- VanDecar, J. C., D. E. James, and M. Assumpção, Seismic evidence for a fossil mantle plume beneath South America and implications for plate driving forces, *Nature*, 378, 25–31, 1995.
- van der Lee, S., D. E. James, and P. G. Silver, Upper mantle *S* velocity structure of central and western South America, *J. Geophys. Res.*, 106, 30,821–30,834, 2001.
- Vdovin, O., J. A. Rial, A. L. Levshin, and M. H. Ritzwoller, Group-velocity tomography of South America and the surrounding oceans, *Geophys. J. Int.*, 136, 324–340, 1999.
- Vidale, J. E., and H. M. Benz, Upper-mantle seismic discontinuities and the thermal structure of subduction zones, *Nature*, 356, 678–683, 1992.
- Weidner, D. J., and E. Ito, Mineral physics constraints on a uniform mantle composition, in *High-Pressure Research in Mineral Physics*, edited by M. H. Manghnani and Y. Syono, pp. 269–274, Terra Sci., Tokyo, 1987.
- Wicks, C. W., and M. A. Richards, A detailed map of the 660-kilometer discontinuity beneath the Izu-Bonin subduction zone, *Science*, 261, 1424–1427, 1993.
- Widiyantoro, S., Studies of seismic tomography on regional and global scale, Ph.D. thesis, Aust. Natl. Univ., Canberra, A. C. T., Australia, 1997.
- Yuan, X., et al., Subduction and collision processes in the Central Andes constrained by converted seismic phases, *Nature*, 408, 958–961, 2000.

S. S. Gao and K. H. Liu, Department of Geology, Kansas State University, 108 Thompson Hall, Manhattan, KS 66506-3201, USA. (sgao@ksu.edu; liu@ksu.edu)

P. G. Silver, Department of Terrestrial Magnetism, Carnegie Institution of Washington, 5241 Broad Branch Road, N.W., Washington, DC 20015, USA. (silver@dtm.ciw.edu)

Y. K. Zhang, Department of Civil and Environmental Engineering, University of California, Berkeley, CA 94720, USA. (yyzhang@uclink.berkeley.edu)